Optical and Quantum Electronics (2022) 54:300
https://doi.org/10.1007/s11082-022-03667-y

Comparison of supercontinuum spectrum generating by hollow core PCFs filled with nitrobenzene with different lattice types

L. Chu Van[1] · T. Nguyen Thi[2] · D. Hoang Trong[2] · B. T. Le Tran[1] · N. Vo Thi Minh[1] · T. Dang Van[1] · T. Le Canh[1] · Q. Ho Dinh[1] · K. Doan Quoc[3]

Received: 22 August 2021 / Accepted: 8 March 2022

Abstract
Three types of hollow-core photonic crystal fibers (HC-PCFs) of optimized design with respect to both chromatic dispersion and loss were used to investigate supercontinuum generation (SCG). The optical properties of HC-PCFs filled with nitrobenzene ($C_6H_5NO_2$) with the circular lattice (CL), square lattice (SL), and hexagonal lattice (HL) are analyzed to choose the optimal fiber. As a result, the three optimized structures: #CF_1 (lattice constant (Λ) of 1.0 μm, filling factor (f_1) of 0.65, and core diameter (D_c) of 1.285 μm), #SF_2 ($\Lambda = 1.0$ μm, $f_1 = 0.7$, and $D_c = 1.23$ μm), #HF_3 ($\Lambda = 1.0$ μm, $f_1 = 0.45$, and $D_c = 1.505$ μm) with flat and close to zero chromatic dispersion curve in the investigated wavelength region, have the values of chromatic dispersion − 10 ps.nm^{-1}.km^{-1} at 1.15 μm, − 7.7 ps.nm^{-1}.km^{-1} at 1.23 μm, and − 3.0 ps nm^{-1} km^{-1} at the 1.55 μm pump wavelength, respectively are intended for SCG in an all-normal dispersion regime. We demonstrate the possibility of coherent octave-wide SCG in the wavelength range of $0.72 \div 1.7$ μm, $0.74 \div 1.77$ μm, and $0.83 \div 2.36$ μm with 90 fs pulses and 10 pJ of low energy in-coupled into the considered fibers core. The obtained results show that SCG with HL-PCFs has the highest efficiency, although all fibers are examined with the same input energy. Especially, the supercontinuum (SC) spectral bandwidth is independent of the type of lattice at the pump energy of 1.57 pJ, and this can be seen as a limitation between the pure self-phase modulation and other nonlinear processes contributing to SCG.

Keywords Dispersion · Nitrobenzene · Nonlinear optics · Photonic crystal fibers · Supercontinuum generation

✉ L. Chu Van
chuvanlanh@vinhuni.edu.vn

✉ K. Doan Quoc
doanquockhoa@tdmu.edu.vn

[1] Vinh University, 182 Le Duan, Vinh City, Vietnam

[2] University of Education, Hue University, 34 Le Loi Street, Hue City, Vietnam

[3] Institute of Applied Technology, Thu Dau Mot University, Binh Duong Province, Vietnam

Published online: 17 April 2022

1 Introduction

SCG has been focused by researchers due to its wide range of applications in various fields (Dudley et al. 2006; Tu and Boppart 2013; Fanjoux et al. 2017; Hoang et al. 2018). The SC spectrum can be used in telecommunication, pulse compression, metrology, and spectroscopy (Alfano 2006; Woodward et al. 2009; Petersen et al. 2018) or other fields depending on its suitable qualities as spectral range, bandwidth, intensity (or power), and intensity flatness. Because SCG is a nonlinear process including the optical wave-breaking (OWB), self-phase modulation (SPM), cross-phase modulation (SPM), Raman scattering (SRS), Raman-Kerr scattering (RKS), modulation instability (MI), soliton fission (SF), the Raman-induced frequency shift (RIFS), and dispersive wave generation (DWG),… its performance depends strongly on the nonlinear characteristic of the PCF including HC-PCF (Agrawal 2012) as well as the optical properties of the pump pulse (Dudley and Taylor 2010). There are two ways usually to generate SC. Firstly, SCG is in the anomalous dispersion PCF, i.e., the PCF has zero-dispersion wavelength (ZDW), the pump wavelength is chosen to be larger but closer to ZDW. This mechanism can create a broad SC spectrum with low energy despite the weak coherence spectrum and large noise since the soliton dynamics are extremely sensitive to pump pulse fluctuations (Corwin et al. 2003; Qian et al. 2018; Heidt et al. 2017). Secondly, SCG is in the all-normal dispersion regime. This way is relied on two effects of the fully coherent nonlinearity OWB and SPM (Finot et al. 2008) which innovate the noise and coherence of SCG beyond the anomalous SCG limits (Heidt et al. 2017; Genier et al. 2019). Thus, the way to generate SC spectrum and its qualities depend on the PCF's (Knight et al. 1996; Birks et al. 1997; Buczyński 2004) (or HC-PCF's (Pandey et al. 2020; Sen et al. 2020; Monfared et al. 2013)) properties as dispersion, ZDW, effective mode area, nonlinearity, and confinement loss (Dudley et al. 2006). The SCG will be most effective if the PCF has flat and close to zero chromatic dispersion curve, small effective mode area, low confinement loss, and high nonlinearity (Dudley and Taylor 2010). These features can be controlled by changing the lattice type and structure parameters in the cladding as well as the filling material in the core of PCF (Birks et al. 1997; Buczyński 2004). The lattice is commonly created in cladding with the circular, square, pentagonal, hexagonal type (Pandey et al. 2020; Sen et al. 2020; Monfared et al. 2013; Wang et al. 2020), the materials are gas or liquids owing nonlinearity high enough (Dudley et al. 2006; Fanjoux et al. 2017; Hoang et al. 2018).

Up to now, there is a lot of research works considering the different types of PCF such as CL-PCF with high negative dispersion (Pandey et al. 2020), hexagonal cladding with a rotated-hexagon core in PCF (Sen et al. 2020), low confinement loss in HL-PCFs (Monfared et al. 2013), an ultra-broadband and compact SL-PCFs (Wang et al. 2020),… These works have analyzed the influence of lattice parameters on the characteristics of PCFs for each lattice structure but did not consider their effectiveness in SCG. The recent work (Tran et al. 2020) has investigated the characteristic quantities of the solid-core PCFs with a different lattice structure, but their influence on SCG has not been discussed yet. In addition, the fibers analyzed in this paper exhibit small nonlinear refractive index of the silica solid core, so SCG would not be efficient. Similarly, there are many lattice structures of PCF used for SCG having diversity quality in previous works, however, there is not any confirmation that which one of lattice types and structures will be more effective for SCG. Furthermore, because these PCFs have lattice rings in the cladding with the same diameter as air holes, they can only optimize chromatic dispersion but not the loss.

To overcome the above limitations, in this paper, the HC-PCF infiltrated with nitrobenzene with three different lattice types including CL, SL, and HL were suggested for SCG. We punctuated the influence of the lattice parameters on the optical features of HC-PCFs with these three lattice types to find the optimal one possessing all-normal dispersion. Next, we simulated the SCG of three optimal PCFs and discussed their SC spectrum qualities.

2 Numerical modelling of optical properties

Because of the moderately toxicity (Xu et al. 2008) only, the high nonlinear refractive index $n_2 = 671 \times 10^{-20} m^2 W^{-1}$ at 1.064 μm, relatively low attenuation with respect to other liquids of the nonlinearity, the low vapor pressure at room temperature, and ease of handling (Sutherland et al. 2003), the nitrobenzene is chosen as the filled liquid. Using a commercial Lumerical Model Solution (LMS) software, we designed the various HC-PCFs infiltrated with nitrobenzene. The schematic of the geometrical structure of these PCFs with different lattice types is shown in Fig. 1.

The photonic cladding consists of eight rings of air-holes with the diameter d, the lattice constant Λ and linear filling factor $f = d/\Lambda$. In the numerical simulation, we used the following lattice constants Λ: 1.0 μm, 1.5 μm, 2.0 μm, and 2.5 μm. The lattice parameters in the first ring around the core have the leading influence on the fiber dispersion characteristics, including ZDW. The mode attenuation, even the higher modes are dominated by the other rings (Saitoh et al. 2003). The other rings are mainly responsible for attenuation of the mode, specifically for higher modes. Therefore, we propose a new design to optimize the structure with the first ring has the filling factor $f_1 = d_1/\Lambda$ changing 0.3 to 0.8, with a step of 0.05, in which d_1 is the air holes diameter of the first ring, the remaining rings have a constant filling factor $f_2 = d_2/\Lambda$ of 0.95. The core diameter is determined $D_{core} = 2\Lambda - 1.1\ d_1$, for $\Lambda = 1.0$ μm and $f_1 = 0.8$, the diameter of core is smallest ($D_{coremin} = 1.12$ μm) while the biggest core ($D_{coremax} = 4.34$ μm) is achieved for $\Lambda = 2.5$ μm and $f_1 = 0.3$. The selected range of the parameters corresponds to the technological requirements of the stack-and-draw method commonly which is used for PCF development. As the PCFs are designed with varying the air holes diameter of the first ring, and the air holes of the remaining rings have a constant diameter of 0.95Λ. Therefore, the created PCFs with minimal loss is the advantage of this design, at the same time the structural parameters can be controlled to obtain the desired dispersion. This is absolutely different from previous publications

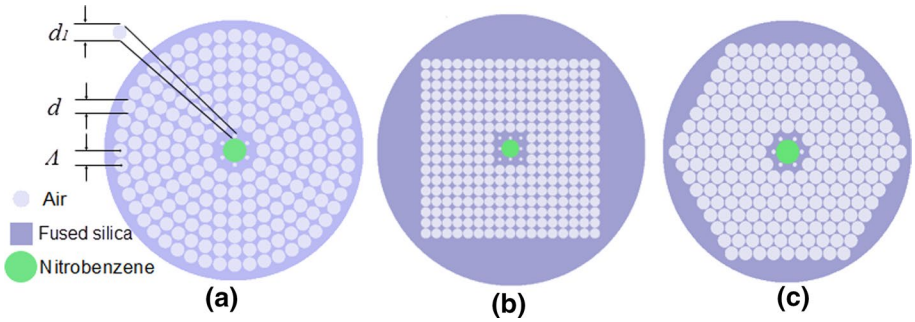

Fig. 1 The geometrical structure of nitrobenzene-core PCFs with **a** CL, **b** SL, and **c** HL

(Hoang et al. 2018; Zhang et al. 2010; Lanh et al. 2017, 2020). In the model, a factor of the constant filling for the first ring was supposed to simplify the PCF's progress in the future. HC-PCFs infiltrated with nitrobenzene can be fabricated using the conventional stack-and-draw method (Hoang et al. 2018, 2019; Pysz et al. 2014). Then, it is selectively filled liquid into the core using thermal fusion splicer (Hoang et al. 2018), or laser writing technique (Vieweg et al. 2010), next, is integrated with a microfluidic pump system to fill liquid into the core (Hoang et al. 2018). We did not confirm whether the select PCF was single-mode or multi-mode. This study was only executed for optimized PCF. The linear refractive index of nitrobenzene (Kedenburg et al. 2012) and fused silica (Tan 1998) as a function of the wavelength can be described by using the Sellmeier formula:

$$n^2(\lambda) = B_0 + \frac{B_1\lambda^2}{\lambda^2 - C_1} + \frac{B_2\lambda^2}{\lambda^2 - C_2} + \frac{B_3\lambda^2}{\lambda^2 - C_3}. \quad (1)$$

In both cases the wavelength λ has dimensions of micrometers (μm) and the respective parameters $B_0 \ldots B_3$ and $C_1 \ldots C_3$ are listed in Table 1.

Figure 2 display the real components of the refractive index of nitrobenzene and fused silica. From the plot, the refractive index of nitrobenzene is always bigger than the refractive index of fused silica. Therefore, light propagates in the nitrobenzene-core PCFs by exploiting the modified total internal reflection mechanism as in the conventional optical fibers. The chromatic dispersion, D of nitrobenzene-core PCFs consists of the waveguide and material dispersion. It is determined as the following equation (Buczyński 2004):

$$D = -\frac{\lambda}{c}\frac{d^2\left(\mathrm{Re}\left[n_{\mathrm{eff}}\right]\right)}{d\lambda^2}, \quad (2)$$

$\mathrm{Re}[n_{\mathrm{eff}}]$ is the real component of the effective refractive index of a guided mode.

The preliminary simulation for important characteristics of HC-PCFs infiltrated with nitrobenzene such as the chromatic dispersion, effective mode area, and loss with different values of lattice constant and diameter of air-holes is implemented by using the

Table 1 Sellmeier's coefficients

Parameters	Values
Nitrobenzene	
B_0	1
B_1	1.30628
B_2	0.00502
C_1	0.02268 μm^2
C_2	0.18487 μm^2
Fused silica	
B_0	1
B_1	0.6694226
B_2	0.4345839
B_3	0.8716947
C_1	4.4801×10^{-3} μm^2
C_2	1.3285×10^{-2} μm^2
C_3	95.341482 μm^2

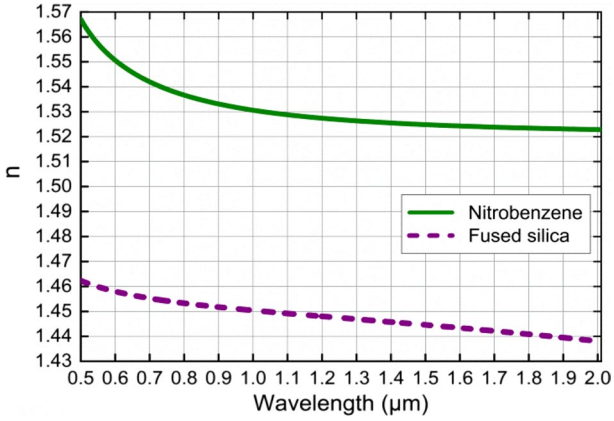

Fig. 2 The real components of the refractive index of nitrobenzene and fused silica

finite-difference eigenmode method with a commercial LMS. The chromatic dispersion characteristics of HC-PCFs infiltrated with nitrobenzene with different lattice types, various values of the lattice constant, and filling factors are presented in Figs. 3, 4, 5 and 6.

For the small core (Λ = 1 μm), the chromatic dispersion is noticeably shifted with changing of Λ and f_1. Two ZDWs were observed in the three types of surveyed PCF corresponding to different values $f_1, f_1 \geq 0.7$ with CL PCFs, $f_1 \geq 0.75$ for SL PCFs, and $f_1 \geq 0.5$ with HL PCFs. The chromatic dispersion is all-normal when $f_1 \leq 0.65$ in CL PCFs, $f_1 \leq 0.7$ for SL PCFs, and $f_1 \leq 0.45$ with HL PCFs, (Fig. 3). Meanwhile, the PCFs with a larger core ($\Lambda \geq 1.5$ μm) has the moderate shift of the chromatic dispersion, they have anomalous dispersions with $\lambda > 1$ μm (Figs. 4, 5 and 6) due to the negative effects of the material dispersion of nitrobenzene. The chromatic dispersion is one of the significant keys for the SCG, the PCF with the flat dispersion allows to obtain the broader SCG (Hoang et al. 2018; Genier et al. 2019). Thus, finding the PCF with the flat near-zero dispersion, and the compatibility of ZDW to the pump wavelength is one of our primary goals. At the same time, we compare the SCG spectrums expansion in HC-PCFs infiltrated with nitrobenzene with different lattice types in the claddings so we choose three PCFs operating in all-normal dispersion region with the flat near-zero dispersion for detailed analysis of SCG. #CF_1, #SF_2, and #HF_3 are the name of these PCFs, their respective structure parameters are shown in Table 2.

Three structures #CF_1, #SF_2, and #HF_3 with lattice constant Λ = 1 μm are chosen since they can offer the flat all-normal dispersion but they have a smaller core than that of other ones. The small core can result in a high confinement loss at the long-wavelength range, i.e., it reduces the spectral broadening, brightness of SG in the long-wavelength range, and effective mode area (Rostami and Soofi 2011). However, we interest-only all-normal dispersion and comparison of SC spectrum generated from the chosen PCFs, the above disadvantages will not consider in this study.

The chromatic dispersion characteristics of the fundamental mode for #CF1, #SF2, and #HF3 are presented in Fig. 7a. Those fibers are intended for SCG in an all-normal dispersion regime with the chromatic dispersion is about -10 $ps.nm^{-1}.km^{-1}$, -7.7 $ps.nm^{-1}.km^{-1}$, and -3.0 $ps.nm^{-1}.km^{-1}$ at the pump wavelength of 1.15 μm, 1.23 μm, and 1.55 μm, respectively. Figure 7b exposes the attenuation characteristics of the basic mode for chosen PCFs. It is clear that the difference between them is negligible, those are characterized mainly by the bulk material losses of nitrobenzene. At the pump wavelength mentioned above, the

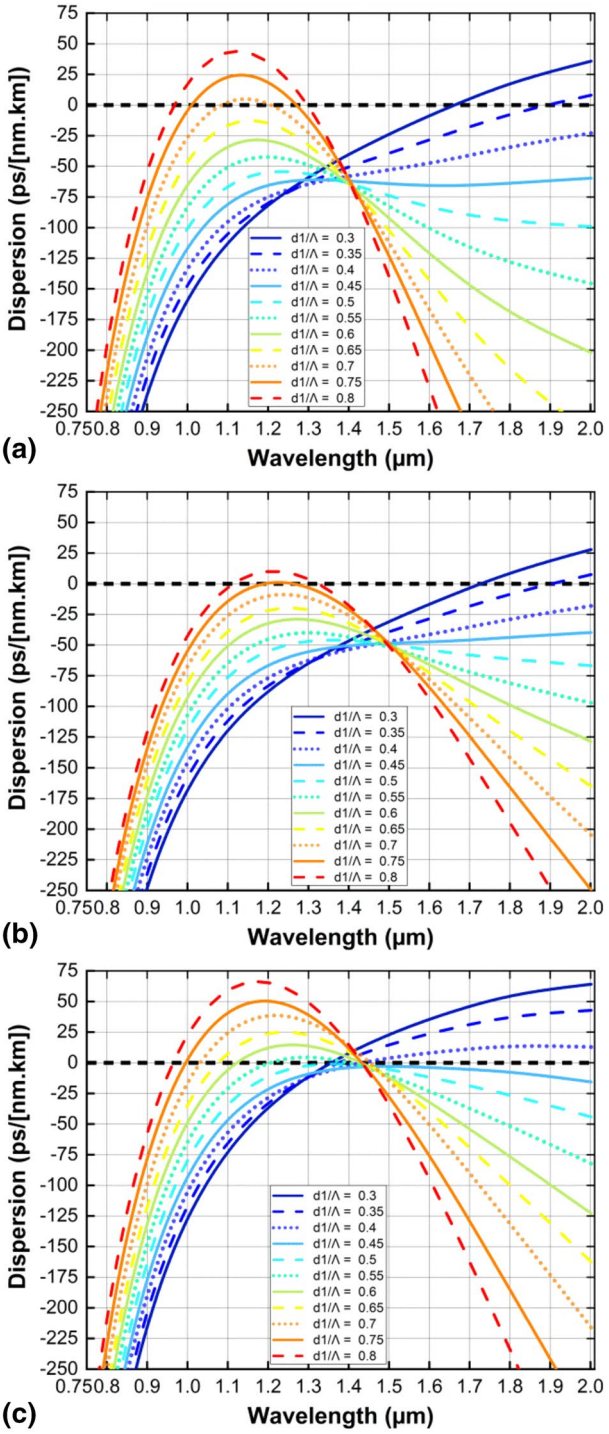

Fig. 3 Characteristics of chromatic dispersion of the fundamental mode for HC-PCFs infiltrated with nitrobenzene with different lattice type: **a** CL, **b** SL, and **c** HL with $\Lambda = 1$ μm, $f_1 = 0.3 \div 0.8$

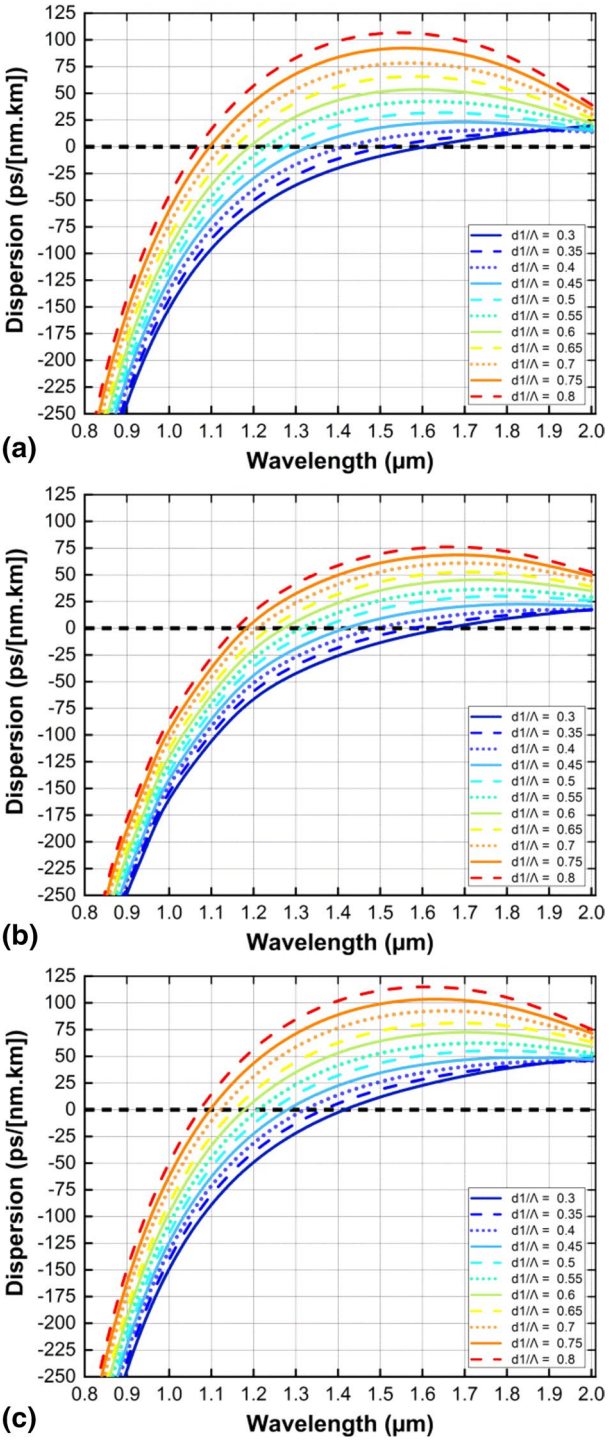

Fig. 4 Characteristics of chromatic dispersion of the fundamental mode for HC-PCFs infiltrated with nitrobenzene with different lattice type: **a** CL, **b** SL, and **c** HL with $\Lambda = 1.5$ μm, $f_1 = 0.3 \div 0.8$

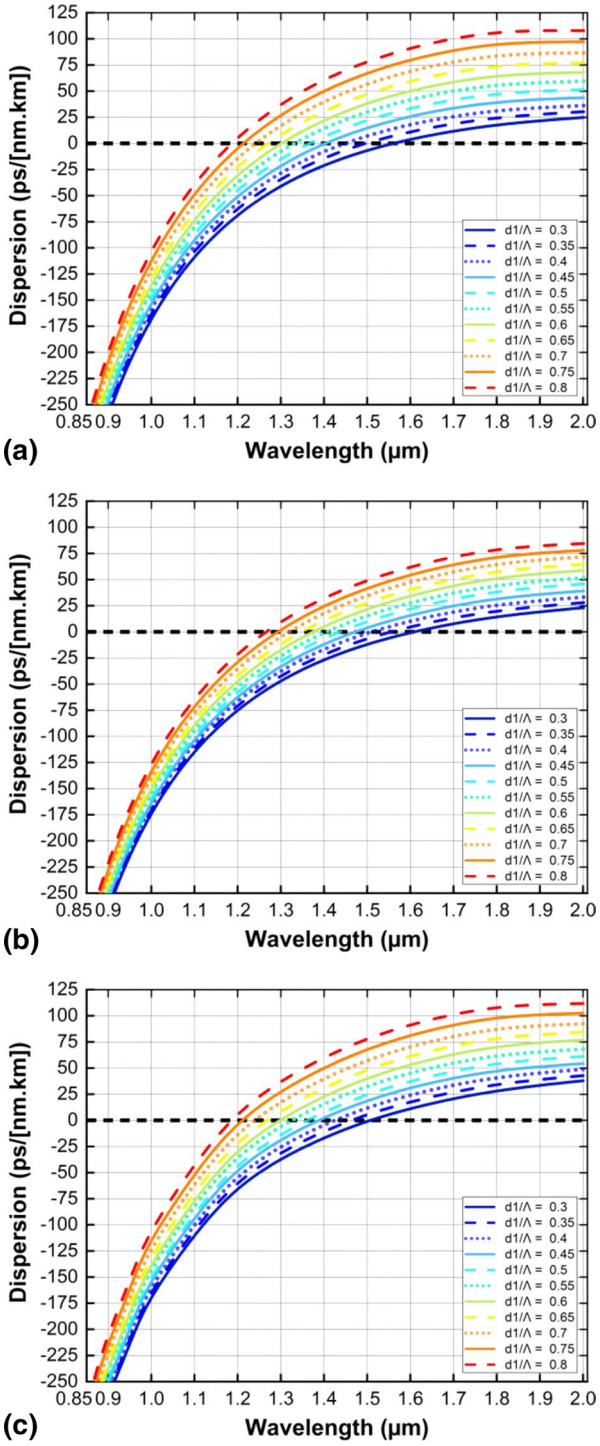

Fig. 5 Characteristics of chromatic dispersion of the fundamental mode for HC-PCFs infiltrated with nitrobenzene with different lattice type: **a** CL, **b** SL, and **c** HL with $\Lambda = 2.0$ μm, $f_1 = 0.3 \div 0.8$

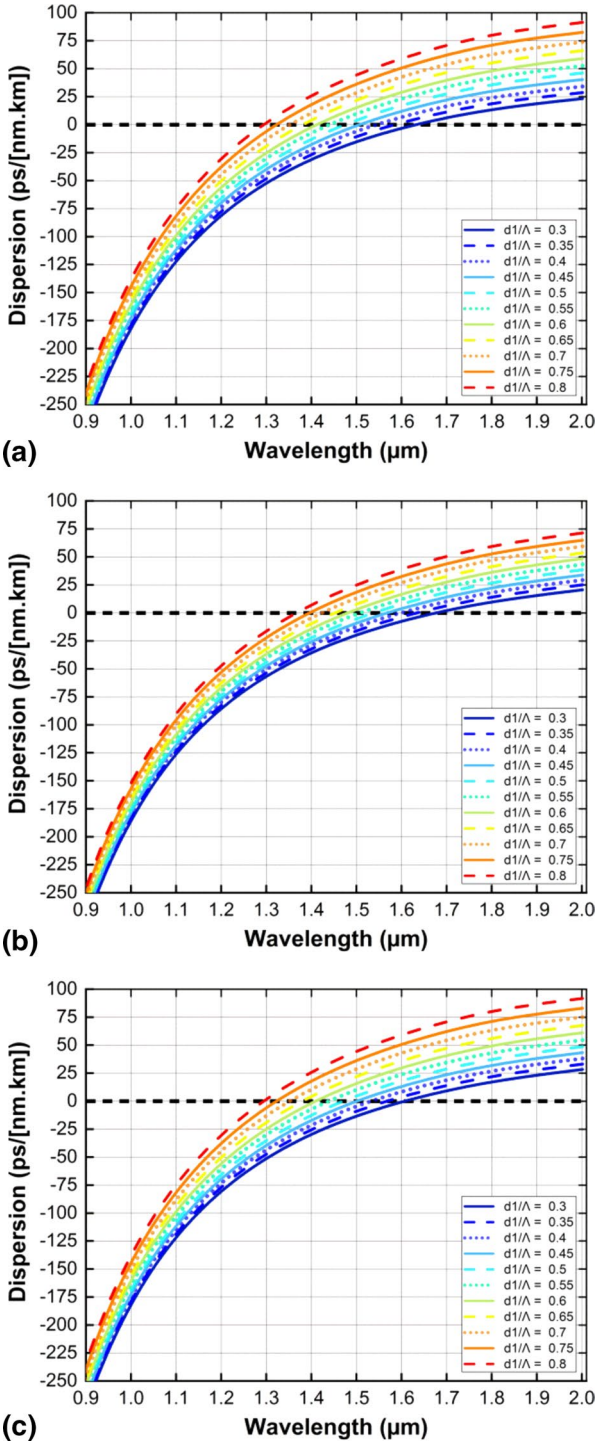

Fig. 6 Characteristics of chromatic dispersion of the fundamental mode for HC-PCFs infiltrated with nitrobenzene with different lattice type: **a** CL, **b** SL, and **c** HL with $\Lambda = 2.5$ μm, $f_1 = 0.3 \div 0.8$

Table 2 The structure parameters of selected HC-PCFs infiltrated with nitrobenzene

#	Type	Λ (μm)	f	D_c (μm)
#CF_1	CL	1.0	0.65	1.285
#SF_2	SL	1.0	0.7	1.23
#HF_3	HL	1.0	0.45	1.505

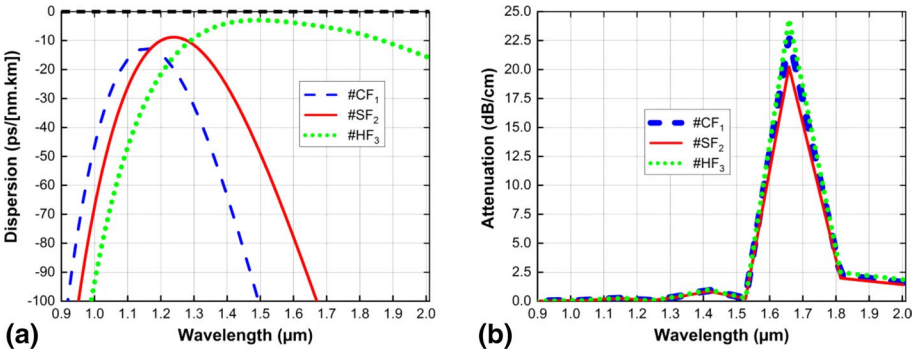

Fig. 7 The **chromatic** dispersion **a** and attenuation **b** characteristics of the fundamental mode inside #CF_1, #SF_2, and #HF_3

attenuation of #CF_1, #SF_2, and #HF_3 are 0.3, 0.2, and 4.42 dB/cm, respectively, which are very low in comparison to that at the wavelength of 1.66 μm. The effective index (n_{eff}), effective mode area (A_{eff}) and nonlinear coefficient ($\gamma = 2\pi n_2/(\lambda A_{eff})$) of the basic mode for the selected PCFs are simulated, and indicated in Fig. 8a, Fig. 8b and Fig. 8c.

Figure 8 evinces that the optical properties of the #CF_1 and #SF_2 versus wavelength are similar but they are significantly different from #HF_3. The bigger effective index and effective mode area of the #HF_3 leads to its smallest nonlinear coefficient. This can be explained that the core diameter of the #HF_3 is larger than those of #CF1 and #SF2. The optical properties corresponding to the pump wavelength of PCFs are certified in Table 3.

3 SCG in proposed fiber

The evolution of the pulses propagating in the investigated fibers is numerically calculated solving the generalised nonlinear Schrödinger equation, using the symmetric split-step Fourier transform method (Dudley and Taylor 2010):

$$\partial_z \tilde{A} - i\tilde{\beta}(\omega)\tilde{A} - \frac{\tilde{\alpha}(\omega)}{2}\tilde{A} = i\gamma\left(1 + \frac{\omega - \omega_0}{\omega_0}\right)\tilde{A}F\left[\int_{-\infty}^{\infty} R(T')|A|^2(T - T')dT'\right], \quad (3)$$

$\tilde{A}(\omega)$ is the Fourier transform of the pulse envelope $A(t)$. The left side of Eq. (3) describes the linear propagation effects which are determined from the attenuation and chromatic dispersion of the fiber, $\tilde{\beta}(\omega) = \beta(\omega) - \beta_0(\omega) - \omega \frac{\partial \beta}{\partial \omega}\Big|_{\omega=\omega_0}$. The right-hand side of the equation depicts the nonlinear effects which depend on the nonlinear optical response of nitrobenzene

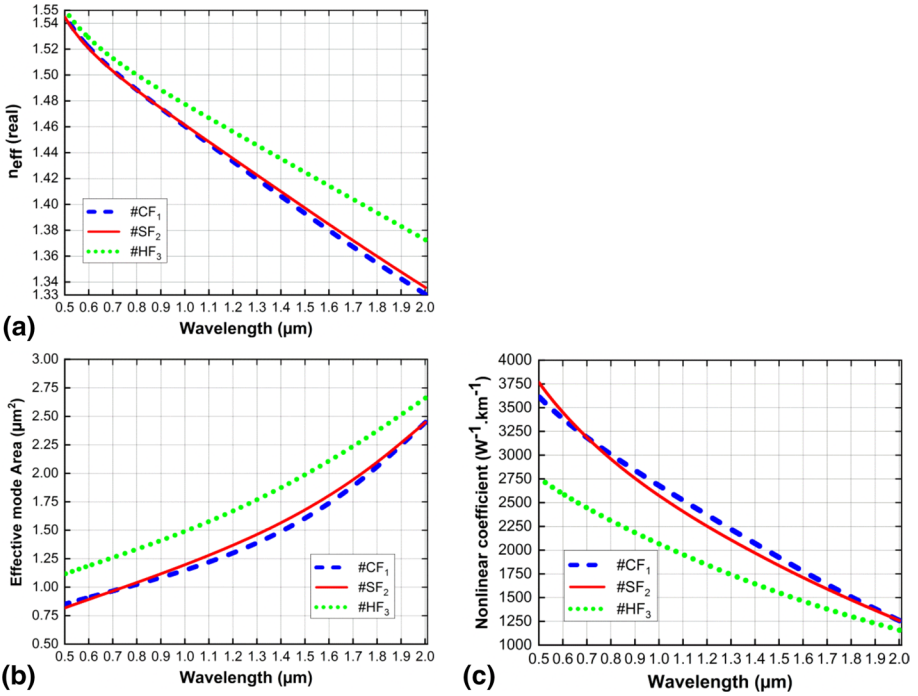

Fig. 8 Characteristics of **a** effective refractive index, **b** effective mode area, and **c** nonlinear coefficient of the fundamental mode for $\#CF_1$, $\#SF_2$, and $\#HF_3$

Table 3 The optical properties of the selected PCFs and those previously published

Fibers with all-normal dispersion	D_c (μm)	Pump wavelength (μm)	D (ps.nm^{-1}.km^{-1})	Attenuation (dB/cm)	A_{eff} (μm^2)	Γ (W^{-1} km^{-1})
Zhao et al. 2018)	1.285	1.03	− 24	0	1.5	1290
Lanh et al. 2017)	3.34	1.55	− 9.46	1.92	7.8	1200
Lanh et al. 2020)	2.34	1.56	− 2.2	2.4	4.73	2000
$\#CF_1$	1.285	1.15	− 31.8	0.3	1.38	2220
$\#SF_2$	1.23	1.23	− 10.7	0.3	1.46	2107
$\#HF_3$	1.505	1.55	− 3.0	4.42	2.04	1742

that is identified by the combination of the bound-electronic and nuclear contribution. Table 4 depicts the nonlinear parameters of these contributions, in which the subscripts *el, d, l* and *c* indicate the bound-electronic, molecular reorientation, molecular interaction, and collision-induced, respectively. τ_r and τ_f are rise time and fall time. The Raman response function in Eq. (3) is given by Agrawal (2012):

$$R(t) = \left(1 - f_R\right)\delta(t) + f_R R'(t), \tag{4}$$

Table 4 The nonlinear parameters used in these simulations (Zhao et al. 2018)

Parameters	Values	Parameters	Values
$n_{2,el}$	0.6×10^{-19} m^2/W	$n_{2,l}$	1.7×10^{-19} m^2/W
$n_{2,d}$	5.0×10^{-19} m^2/W	$n_{2,c}$	0.35×10^{-19} m^2/W
$\tau_{r,d}$	0.1 ps	$\tau_{r,c}$	0.2 ps
$\tau_{f,d}$	3.5 ps	$\tau_{f,c}$	0.1 ps
		$\tau_{f,l}$	0.4 ps

here f_R is a part of the delayed contribution, which is a fraction of nuclear contribution to the nonlinear optical response of nitrobenzene. Based on Table 4, f_R of nitrobenzene is around 0.87. $\delta(t)$ is the Dirac delta function. $R'(t)$ represents the delayed nonlinear response, is a sum of the electronic-bound and molecular contribution mechanisms which is able to be defined as in the following equation (Zhang et al. 2010):

$$R(t') = \frac{1}{N}\left[2n_{el} + \left(n_{2l}C_{21}e^{-t'/t_{fl}}\int_0^\infty \frac{\sin(\omega t')}{\omega}g(\omega)d\omega + \sum_{k=c,d} n_{2k}C_{2k}\left(1-e^{-t'/t_{rk}}\right)\Theta(t')\right)\right], \tag{5}$$

where $N = n_{2el} + n_{2c} + n_{2d} + n_{2l}$, and the values of $n_{2,el}$, $n_{2,d}$, $\tau_{r,d}$, $\tau_{f,d}$, $n_{2,l}$, $n_{2,c}$, $\tau_{r,c}$, $\tau_{f,c}$, $\tau_{f,l}$ are defined in the Table 4.

In our numerical modeling, coefficients of the high-order chromatic dispersion are calculated through the expansion coefficients of the Taylor series of the propagation constant at the pumping pulse frequency. Coefficients of the high order chromatic dispersion are shown in Table 5.

The SCG coherence is confirmed by using the first-order coherence according to Eq. (6) (Dudley et al. 2006; Dudley and Taylor 2010):

$$\left|g_{12}^{(1)}(\omega)\right| = \left|\frac{\left\langle \tilde{A}_i^*(\omega)\tilde{A}_j(\omega)\right\rangle_{i=j}}{\left[\left\langle\left|\tilde{A}_i(\omega)\right|^2\right\rangle\left\langle\left|\tilde{A}_j(\omega)\right|^2\right\rangle\right]^{1/2}}\right|. \tag{6}$$

Table 5 The coefficients of high order chromatic dispersion at the pump wavelength

Coefficient	#CF_1	#SF_2	#HF_3
β_2 (ps^2/m)	2.79×10^{-2}	9.23×10^{-3}	3.99×10^{-3}
β_3 (ps^3/m)	-2.43×10^{-4}	-8.32×10^{-5}	-2.11×10^{-5}
β_4 (ps^4/m)	1.85×10^{-6}	1.26×10^{-6}	2.34×10^{-7}
β_5 (ps^5/m)	-7.93×10^{-9}	-4.28×10^{-9}	7.01×10^{-10}
β_6 (ps^6/m)	4.46×10^{-11}	-1.95×10^{-12}	3.25×10^{-11}
β_7 (ps^7/m)	-2.47×10^{-14}	-1.20×10^{-12}	-6.61×10^{-13}
β_8 (ps^8/m)	-1.05×10^{-14}	2.44×10^{-14}	2.68×10^{-15}
β_9 (ps^9/m)	9.31×10^{-14}	4.63×10^{-16}	-1.75×10^{-17}
β_{10} (ps^{10}/m)	2.72×10^{-18}	-1.72×10^{-17}	6.48×10^{-19}
β_{11} (ps^{11}/m)	-4.88×10^{-20}	-4.97×10^{-20}	3.93×10^{-20}

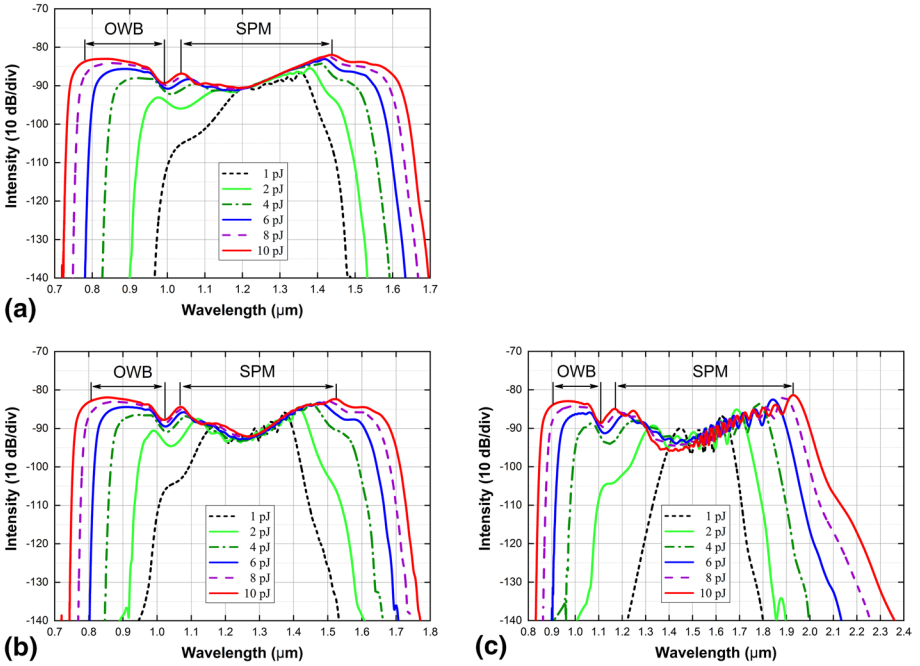

Fig. 9 The spectral intensity of SCG in #CF_1, #SF_2, and #HF_3 fibers with 90 fs duration, 5 cm fiber length, and different pulse energies in the range of $1 \div 10$ pJ: **a** #CF_1, **b** SF_2, and **c** #HF_3

In the simulations, the laser pulses are modeled by a Gaussian pulse that is centered at the pump wavelength, are represented in Eq. (7):

$$A(t) = \sqrt{P_0} \exp\left(-\frac{t^2}{2t_0^2}\right). \tag{7}$$

The pump pulses have the central wavelength (λ_p) of 1.15 μm, 1.23 μm, and 1.55 μm, corresponding to #CF_1, #SF_2, and #HF_3 with the duration (τ) of 90 fs. The progression of the SC is simulated for a propagational distance of 5 cm with the input different pump energies (E) in the range of $1 \div 10$ pJ, which is corresponding to the peak power (P_0) in the range of $11 \div 111$ W. The SC spectrum is quoted in Fig. 9. The results show that: (1) Since the #CF_1, #SF_2, and #HF_3 exist the all-normal dispersion, the main effects that dominate the SC spectrum are the SPM and OWB in both edges. (2) For the input pump energy lower than 2 pJ (next, we will denote exactly 1.57 pJ), the SPM plays a key role in the broadening of the spectrum. (3) If the input pump energy is higher than 2 pJ, the other nonlinear processes contribute to the SC spectrum in the middle, consequently the spectrum consists of the peaks. (4) The combination of SPM and OWB with other nonlinear processes results in the outermost intense peaks. (5) The OWB begins to occur when the input pump energy increases more than 2 pJ, which makes the spectrum wider rapidly. 6) With the same value of the pump energy, the flatness of the spectral intensity is not significantly reduced and the SC spectral bandwidth increases noticeably from #CF_1 to #SF_2 and then #HF_3. This increase can be explained based on the large range wavelength of all-normal

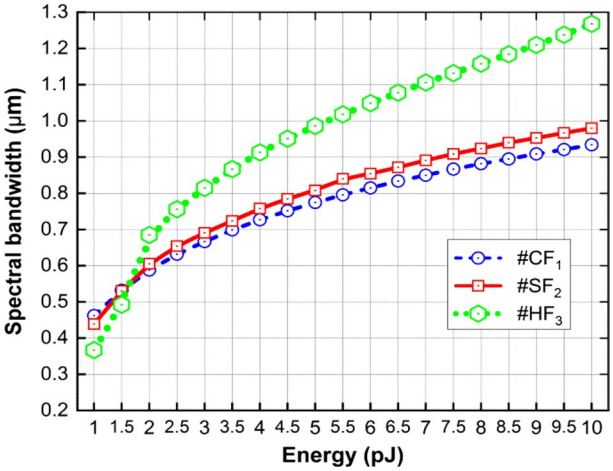

Fig. 10 The spectral bandwidth vs pump energies

Table 6 The SC spectral bandwidth for our models in comparison to HL-PCFs with all-normal dispersion with different liquids

Liquid	τ (fs)	E (nJ)	P (kW)	λ_p (μm)	Fiber length (cm)	SC range (μm)	SCSB (μm)	Regime	Ref
C_7H_8	350	2.5	7.14	1.55	5	1.10 ÷ 1.75	0.65	Normal	Lanh et al. 2017)
$C_6H_5NO_2$	90	0.5	5.56	1.56	5	0.80 ÷ 2.10	1.3	Normal	Lanh et al. 2020)
$CHCl_3$	400	1.0	2.50	1.03	20	0.60 ÷ 1.26	0.66	Normal	Lanh et al. 2019)
C_7H_8	18,000	200	11.11	0.532	60	0.55 ÷ 0.87	0.32	Normal	Fanjoux et al. 2017)
CS_2	180	2.55	14.17	1.91	16	1.79 ÷ 2.40	0.61	Normal	Churin et al. 2013)
C_7H_8	400	10	25.00	1.03	10	0.95 ÷ 1.10	0.25	Normal	Hoang et al. 2018)
CCl_4	300	0.8	2.67	1.064	30	0.95 ÷ 1.15	0.2	Normal	Ho et al. 2018)
CCl_4	400	25	62.50	1.03	20	0.85 ÷ 1.25	0.4	Normal	Hoang et al. 2019)
$C_6H_5NO_2$	90	0.01	0.111	1.15	5	0.72 ÷ 1.70	0.934	Normal	$\#CF_1$
$C_6H_5NO_2$	90	0.01	0.111	1.23	5	0.74 ÷ 1.77	0.98	Normal	$\#SF_2$
$C_6H_5NO_2$	90	0.01	0.111	1.55	5	0.83 ÷ 2.36	1.268	Normal	$\#HF_3$

dispersion (see Fig. 7a). The dependence of SC spectral bandwidth (SCSB) at the intensity of − 110 dB the input pump energy is presented in Fig. 10.

As it is seen from Fig. 10, the SC spectral bandwidth increases with the growth of input pump energy, and conversely. At the input pump energy of 1.57 pJ, this value is about 0.55 μm for all proposed PCFs. If the input pump energy is lower than 1.57 pJ, the

increasing rate of the SC spectral bandwidth is lowest for the $\#HF_3$, higher for $\#SF_2$, and highest for $\#CF_1$, however, we observe the reverse when the input energy is large enough (greater than 1.57 pJ). This feature shows the dominant role of SPM at the input pump energy lower than 1.57 pJ (not 2 pJ as discussed above), while the OWB and other nonlinear processes represent outstanding contributions at the higher input pump energy than 1.57 pJ. Thus, for our proposed PCFs, the input pump energy of 1.57 pJ can be seen as critical, at which the SC spectral bandwidth does not depend on the lattice type. At 10 pJ of input pump energy, the SC spectral bandwidth for $\#CF_1$, $\#SF_2$, and $\#HF_3$ are 0.934 μm, 0.980 μm, and 1.268 μm, respectively, which are comprised that of previous works in Table 6.

From Table 6, we see that the SC spectral bandwidth for the $\#HF_3$ is widest and comparable to one reported in Ref. (Lanh et al. 2020). This means that the PCF with hexagonal structure is most effective for the SCG in the broadening means.

4 Conclusions

The optical properties as the effective refractive index, chromatic dispersion, effective mode area, and consequently the nonlinear coefficient of nitrobenzene-core PCF were analyzed in detail. We have investigated the dependence of those optical properties on the lattice types, lattice constant, and filling factor to optimize three structures: $\#CF_1$ ($\Lambda = 1.0$ μm, $f_1 = 0.65$, and $D_c = 1.285$ μm), $\#SF_2$ ($\Lambda = 1.0$ μm, $f_1 = 0.7$, and $D_c = 1.23$ μm), $\#HF_3$ ($\Lambda = 1.0$ μm, $f_1 = 0.45$, and $D_c = 1.505$ μm). These PCFs have flat and close to zero chromatic dispersion curve in the investigated wavelength region, have the values of chromatic dispersion -10 ps nm^{-1} km^{-1} at 1.15 μm, -7.7 ps nm^{-1} km^{-1} at 1.23 μm, and -3.0 ps nm^{-1} km^{-1} at 1.55 μm of the pump wavelength, respectively, are intended for SCG in an all-normal regime of the chromatic dispersion. The high nonlinear coefficient is obtained at the pump wavelength, whose values are 2220 W^{-1} km^{-1}, 5155 W^{-1} km^{-1}, and 5035 W^{-1} km^{-1} of $\#CF_1$, $\#SF_2$ and $\#HF_3$, respectively. The above advantages of optimal PCFs are considered for simulation SCG using the pump pulse with the energy of 10 pJ and the duration of 90 fs. The achieved SC spectrums has the relative flat intensity with the spectral range of $0.72 \div 1.7$ μm, $0.74 \div 1.77$ μm, and $0.8 \div 2.36$ μm in 10 dB dynamics, respectively. The nonlinear processes occurring in normal regimes SCG are like the ones that exist in the other PCFs with highly nonlinear liquids-filled cores (Fanjoux et al. 2017; Hoang et al. 2018; Lanh et al. 2017, 2020, 2019; Tan 1998; Zhao et al. 2018; Churin et al. 2013). The obtained results clearly demonstrate that the hexagonal lattice PCFs for SC applications have the highest efficiency. There are two main obtained results be seen as advantages: (i) The PCF with the hexagonal lattice of the cladding is most effective to broaden the SC spectral in comparison to other ones. (ii) Existence a critical input pump energy, at which SC spectral bandwidth did not depends on the lattice type of the cladding. This critical input pump energy (i.e., critical power) will be considered as a top limit for the pure self-phase modulation, and down limit for the nonlinear processes. This could be a hint towards the choice of experimental data to examine the SCG in future studies.

Acknowledgements This research is funded by Vietnam National Foundation for Science and Technology Development (NAFOSTED) under grant number 103.03-2020.03; Vietnam's Ministry of Education and Training (B2021- DHH-08).

References

Agrawal, G.: Nonlinear Fiber Optics. Academic Press, Cambridge (2012)

Alfano, R.R.: The ultimate white light. Sci. Am. **295**, 86–93 (2006)

Birks, T.A., Knight, J.C., Russell, P.S.J.: Endlessly single-mode photonic crystal fiber. Opt. Lett. **22**, 961–963 (1997)

Buczyński, R.: Photonic crystal fibers. Acta Phys. Pol. A **106**, 141–168 (2004)

Churin, D., Nguyen, T.N., Kieu, K., Norwood, R.A., Peyghambarian, N.: Mid-IR supercontinuum generation in an integrated liquid core optical fiber filled with CS2. Opt. Mater. Express **3**, 1358–1364 (2013)

Corwin, K.L., Newbury, N.R., Dudley, J.M., Coen, S., Diddams, S.A., Weber, K., Windeler, R.S.: Fundamental Noise Limitations to Supercontinuum Generation in Microstructure Fiber. Phys. Rev. Lett. **90**, 113904 (2003)

Dudley, J.M., Genty, G., Coen, S.: Supercontinuum generation is photonic crystal fiber. J. Rev. Mod. Phys. **78**, 1135–1184 (2006)

Dudley, J.M., Taylor, J.R.: Supercontinuum Generation in Optical Fibers. Cambridge University Press, Cambridge (2010)

Fanjoux, G., Margueron, S., Beugnot, J.C., Sylvestre, T.: Supercontinuum generation by stimulated Raman-Kerr scattering in a liquid core optical fiber. J. Opt. Soc. Am. B **34**, 1677–1683 (2017)

Finot, C., Kibler, B., Provost, L., Wabnitz, S.: Beneficial impact of wave-breaking for coherent continuum formation in normally dispersive nonlinear fibers. J. Opt. Soc. Am. B **25**, 1938–1948 (2008)

Genier, E., Bowen, P., Sylvestre, T., Dudley, J.M., Moselund, P., Bang, O.: Amplitude noise all-normal dispersion coherence degradation of femtosecond supercontinuum generation in all normal-dispersion fibers. J. Opt. Soc. Am. B **36**, A161–A167 (2019)

Heidt, A.M., Feehan, J.S., Price, J.H.V., Feurer, T.: Limits of coherent supercontinuum generation in normal dispersion fibers. J. Opt. Soc. Am. B **34**, 764–775 (2017)

Ho, D.Q., Pniewski, J., Le, V.H., Ramaniuk, A., Cao, L.V., Borzycki, K., Khoa, D.X., Klimczak, M., Buczyński, R.: Optimization of optical properties of photonic crystal fibers infiltrated with carbon tetrachloride for supercontinuum generation with subnanojoule femtosecond pulses. Appl. Opt. **57**, 3738–3746 (2018)

Hoang, V.T., Kasztelanic, R., Anuszkiewicz, A., Stepniewski, G., Filipkowski, A., Ertman, S., Pysz, D., Wolinski, T., Xuan, K.D., Klimczak, M., Buczynski, R.: All-normal dispersion supercontinuum generation in photonic crystal fibers with large hollow cores infiltrated with toluene. Opt. Mater. Express **8**, 3568–3582 (2018)

Hoang, V.T., Kasztelanic, R., Filipkowski, A., Stępniewski, G., Pysz, D., Klimczak, M., Ertman, S., Cao, L.V., Woliński, T.R., Trippenbach, M., Khoa, D.X., Śmietana, M., Buczyński, R.: Supercontinuum generation in an all-normal dispersion large core photonic crystal fiber infiltrated with carbon tetrachloride. Opt. Mater. Express **9**, 2264–2278 (2019)

Kedenburg, S., Vieweg, M., Gissibl, T., Giessen, H.: Linear refractive index and absorption measurements of nonlinear optical liquids in the visible and near-infrared spectral region. Opt. Mat. Express **2**, 1588–1611 (2012)

Knight, J.C., Birks, T.A., Russell, P.S.J., Atkin, D.M.: All-silica single-mode optical fiber with photonic crystal cladding. Opt. Lett. **21**, 1547–1549 (1996)

Lanh, C.V., Anuszkiewicz, A., Ramaniuk, A., Kasztelanic, R., Khoa, D.X., Trippenbach, M., Buczyński, R.: Supercontinuum generation in photonic crystal fibres with core filled with toluene. J. Opt. **19**, 125604 (2017)

Lanh, C.V., Thuy, H.V., Van, C.L., Borzycki, K., Khoa, D.X., Vu, T.Q., Trippenbach, M., Buczyński, R., Pniewski, J.: Optimization of optical properties of photonic crystal fibers infiltrated with chloroform for supercontinuum generation. Laser Phys. **29**, 075107 (2019)

Lanh, C.V., Thuy, H.V., Van, C.L., Borzycki, K., Khoa, D.X., Vu, T.Q., Trippenbach, M., Buczyński, R., Pniewski, J.: Supercontinuum generation in photonic crystal fibers infiltrated with nitrobenzene. Laser Phys. **30**, 035105 (2020)

Monfared, Y.E., Javan, A.R.M., Kashani, A.R.M.: Confinement loss in hexagonal lattice photonic crystal fibers. Optik **124**, 7049–7052 (2013)

Pandey, S.K., Prajapati, Y.K., Maurya, J.B.: Design of simple circular photonic crystal fiber having high negative dispersion and ultra-low confinement loss. Results Opt. **1**, 100024 (2020)

Petersen, C.R., Moselund, P.M., Huot, L., Hooper, L., Bang, O.: Towards a table-top synchrotron based on supercontinuum generation. Infrared Phys. Technol **91**, 182–186 (2018)

Pysz, D., Kujawa, I., Stepien, R., Klimczak, M., Filipkowski, A., Franczyk, M., Kociszewski, L., Buzniak, J., Harasny, K., Buczynski, R.: Stack and draw fabrication of soft glass microstructured fiber optics. Bull. Pol. Acad. Sci. Tech. Sci **62**, 667–682 (2014)

Qian, K., Gu, Z., Xu, J., Dong, X., Yu, W., Yu, Z., Ren, D.: Noise-like pulse erbium-doped fiber laser for supercontinuum generation. Optik **158**, 215–219 (2018)

Rostami, A., Soofi, H.: Correspondence between effective mode area and dispersion variations in defected core photonic crystal fibers. J. Lightwave Technol. **29**, 234–241 (2011)

Saitoh, K., Koshiba, M., Hasegawa, T., Sasaoka, E.: Chromatic dispersion control in photonic crystal fibers: application to ultra-flattened dispersion. Opt. Express **11**, 843–852 (2003)

Sen, S., Shafi, M.A.A., Kabir, M.A.: Hexagonal photonic crystal Fiber (H-PCF) based optical sensor with high relative sensitivity all-normal dispersion low confinement loss for terahertz (THz) regime. Sens. Bio-Sens. Res. **30**, 100377 (2020)

Sutherland, R.L., McLean, D.G., Kirkpatrick, S.: Handbook of Nonlinear Optics. CRC Press, Boca Raton (2003)

Tan, C.Z.: Determination of refractive index of silica glass for infrared wavelengths by IR spectroscopy. J. Non-Cryst. Solids **223**, 158–163 (1998)

Tran, L.T.B., Thuy, N.T., Ngoc, V.T.M., Trung, L.C., Minh, L.V., Van, C.L., Khoa, D.X., Lanh, C.V.: Analysis of dispersion characteristics of solid-core PCFs with different types of lattices in the claddings, infiltrated with ethanol. Photon. Lett. Poland **12**, 106–108 (2020)

Tu, H., Boppart, S.A.: Coherent fiber supercontinuum for biophotonics. Laser Photon. Rev. **7**, 628–645 (2013)

Vieweg, M., Gissibl, T., Pricking, S., Kuhlmey, B.T., Wu, D.C., Eggleton, B.J., Giessen, H.: Ultrafast nonlinear optofluidics in selectively liquid-filled photonic crystal fibers. Opt. Express **18**, 25232–25240 (2010)

Wang, Y., Li, S., Wu, J., Yu, P., Li, Z.: Design of an ultrabroadband and compact filter based on square-lattice photonic crystal fiber with two large gold-coated air holes. Photon. Nanostruct. Fundament. Appl. **41**, 100816 (2020)

Woodward, J.T., Smith, A.W., Jenkins, C.A., Lin, C., Brown, S.W., Lykke, K.R.: Supercontinuum sources for metrology. Metrologia **46**, S277–S282 (2009)

Xu, Y., Chen, X., Zhu, Y.: "High sensitive temperature sensor using a liquid-core optical fiber with small refractive index difference between core and cladding materials. Sensors **8**, 1872–1878 (2008)

Zhang, H., Chang, S., Yuan, J., Huang, D.: Supercontinuum generation in chloroform-filled photonic crystal fibers. Optik **121**, 783–787 (2010)

Zhao, P., Reichert, M., Benis, S., Hagan, D.J., Stryland, E.W.V.: Temporal and polarization dependence of the nonlinear optical response of solvents. Optica **5**, 583–594 (2018)